BCSJ

Document type: Article

A New Heterometallic MOF in Cyanosilylation Reaction, Treatment and Care Management Value in Stroke by Reducing Oxidative Stress Damage

Shu-Rong Chen,[1,#] Yi Li,[2,#] Bi-Yu Wu,[1] and Hui Xu*[3]

[1]Department of Geriatrics, Quanzhou 1st Hospital Affiliated to Fujian Medical University, Quanzhou, Fujian, P. R. China

[2]Department of Thyroid & Breast Surgery, the Fifth Affiliated Hospital, Sun Yat-Sen University, Zhuhai, Guangdong, P. R. China

[3]Department of Fundamental Nursing, The Nursing and Health College of Zhengzhou University, Zhengzhou, Henan, P. R. China

E-mail: hui_xu12@sina.com

Received: September 18, 2019; Accepted: October 19, 2019; Web Released: October 26, 2019

Hui Xu

Hui Xu, M.M., Associate Professor. She worked in the Nursing and Health College of Zhengzhou University. Her research fields focus on health management of stroke and cognitive impairment, health promotion among older adults and health policy of aged-care.

Abstract

By employment the heterometallic strategy, a new highly porous metal-organic framework $\{(Me_2NH_2)[Mn_3K_2(TZIA)_3(H_2O)_3]\cdot(DMF)_4\}_n$ (**1**) was prepared via corresponding K(I)and Mn(II) salts and hetero-donor organic ligand 5-(1H-tetrazol-5-yl)isophthalic acid (H_3TZIA) via solvothermal conditions in water and DMF mixed solvent. X-ray study of a single crystal shows that ionic K^+ was immobilized on the surface of pores via trinuclear Mn^{2+}–tetrazole coordination motif. The resulting activated **1a** has been explored in detail by BET analysis to probe its porosity. The removal of water molecules in order to generate **1a** makes it possible for K^+ ions to be applied as an efficient and size-selective multiphase catalyst for cyanosilylation of acetaldehyde under the mild conditions without solvent. Furthermore, ELISA assay was performed to measure IL-18 and IL-1β level in hCMEC/D3 human brain microvascular endothelial cells after compound treatment. Besides, ROS detection and RT-PCR was performed to detect ROS production as well as the related gene expression. Next, the protective effect of the compound was evaluated in animal model *in vivo*.

Keywords: Hetero-donor organic ligand | Porous framework | Cyanosilylation reaction

1. Introduction

According to the World Health Organization, stroke ranks No. 2 in leading preventable death worldwide and No. 4 in lost productivity, which has been a serious social problem disturbing the everyday life of people.[1,2] Every year, stroke caused deaths of 5.7 million as well as first time illnesses of 16 million, by 2030, those numbers could reach up to 7.8 and 23 million.[3] Despite the fact that over the last decade, stroke mortality has declined due to the use of more targeted preventive drugs, such as statins and antihypertensives, strokes remain a risk factor seriously threatening human health.[4] Thus, in this research, we aimed to explore new candidates with excellent protective activity in stroke treatment and clinical care management.

Porous coordination polymers (PCPs) or metal-organic frameworks (MOFs) are crystalline materials composed of coordination bonds of organic ligands and metal clusters/ions.[5–7] MOFs are well known for their beauty along with presenting diverse structures and catalysis, separation, gas storage, luminescence, sensing, as well as other advanced functions.[8–10] Metal ions in MOFs acting as skeleton connecting sites may be used as the surface of the heterogeneous catalyst to separate Lewis acid sites. Unfortunately, in solution, many MOFs are unstable. Stability is essential for application to industrial processes and recovery of heterogeneous catalysts. Therefore, preparing MOFs with stability remains a great challenge. MOF stability is decided largely by secondary building units (SBUs) or metal ions. The recent literature has revealed that cluster-based units could endow MOFs with better framework stability compared with those based on the single metal ions.[11,12]

Trialkylsilyl cyanide (TMSCN) reaction with carbonyl compounds is an important approach to C-C bond formation in organic synthesis. It can be used for forming derivatives of cyanohydrin, and can also be converted into many pharma-

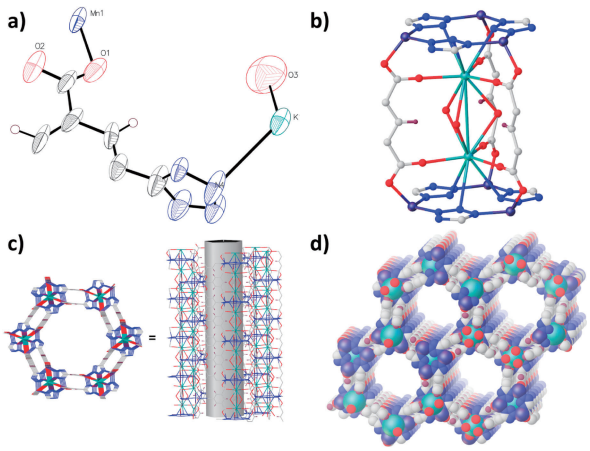

Figure 1. (a) View of asymmetric unit for complex **1**. (b) View of the Mn-K MBB. (c) View of the formation of the 1D channels; (d) The spacing filling mode for the 3D framework of **1**.

ceuticals along with chemicals, for example, β-hydroxy amino alcohols, alpha-hydroxy ketones, alpha-hydroxy acids, etc.[13] Hence, it is an attractive target for chemists to find catalysts with high efficacy for carbonyl compound cyanosilication catalyzed by TMSCN. In recent decades, many of the homogeneous catalysts, such as *N*-heterocyclic carbenes, inorganic or organic salts, Lewis bases and Lewis acids, can catalyze reaction, and they have been widely investigated.[14,15] Nevertheless, the reactions of homogeneous catalysts usually require painstaking purification, so in recent years, research in the field has been mainly focused on the use of the heterogeneous catalysts, particularly MOFs, with the aim of overcoming the problem of product catalyst separation under solvent-free conditions.[16–18] In this study, by employment the heterometallic strategy, a new highly porous metal-organic framework $\{(Me_2NH_2)[Mn_3K_2(TZIA)_3(H_2O)_3]\cdot(DMF)_4\}_n$ (**1**) (Figure 1) was triumphantly prepared via corresponding K(I) and Mn(II) salts and hetero-donor organic ligand 5-(1H-tetrazol-5-yl)isophthalic acid (H_3TZIA) under solvothermal conditions in water and DMF mixed solvent. X-ray diffraction of a single crystal showed that K^+ ions were immobilized on pore surfaces via a trinuclear Mn^{2+}–tetrazole coordination motif. The resulting activated **1a** has been explored in detail by BET analysis to probe its porosity. The removal of water molecules in order to generate **1a** makes it possible for K^+ ions to be applied as an efficient and size-selective multiphase catalyst for solvent-free cyanosilylation of acetaldehyde under mild conditions. In biological research, the protective effect of this new compound was evaluated both *in vitro* and *in vivo*. The ELISA assay of IL-18 and IL-1β indicated inhibition activity of the compound in the inflammatory level in hCMEC/D3 endothelial cells. Besides, the ROS detection and RT-PCR results revealed the compound could also inhibit ROS production via reducing the related gene expression. Finally, *in vivo* study suggested the compound has excellent prevention activity *in vivo*.

2. Results and Discussion

Crystal Structure of Complex 1. In water and DMF mixed solvent, the target complex **1** can be easily acquired with high crystallinity by solvothermal synthesis. On the basis of the crystal data collected under room temperature, the results of refinement along with structural decomposition showed that complex **1** can crystallize in the square $P6_3/m$ space group and has a three-dimensional framework which has nanotube channels. There is one crystallographically independent Mn^{2+} ion, one K^+ ion, one μ_2-bridging water molecule as well as a half $TZIA^{3-}$ ligand in the asymmetric unit. Mn^{2+} ion among molecular units have tetrahedral coordination geometry, which is defined via two O atoms from four independent $TZIA^{3-}$ ligands as well as two N atoms from the tetrazole groups, which forms a distorted tetrahedral coordination environment. Three Mn^{2+} ions were linked by the groups of tetrazolium to form the trinuclear molecular building block (MBB) with triangular shape. N atoms of the group of tetrazolium bind two K^+ ions to trinuclear MBB via coordination and distribute symmetrically on the triangle. K^+ ions are partially linked via isophthalate along with water acid on two independent $TZIA^{3-}$ ligands generating a new MBB. MBBs are bridged via sharing the motifs of Mn^{2+}–tetrazole to provide the building unit with rod-like Co-K. The rod-like structure unit is connected with the coordination of K^+ and Mn^{2+} centers through $TZIA^{3-}$ ligand carboxyl group to provide the porous skeleton which is 1-D hexagonal channels with nanotube-shape (considering Van der Waals radius, pore size = 12 Å). Ignoring the $[(CH_3)_2NH_2]^+$ ions within channels as well as solvent molecules with disorder state, PLATON estimates an achievable volume of 53.2%.

PXRD, TGA and BET Analysis. With the aim of checking the as-prepared complex **1** phase purity, the PXRD pattern of complex **1** was collected at room temperature by using freshly prepared samples, and the results are shown in Figure 2a. The observed along with the calculated diffraction peaks well reflect sample purity. The discrepancy of reflective strength for observed along with simulated results is because of distinct crystal orientation within powder samples. Complex **1** thermogravimetric analysis was carried out and the thermodynamic stability of complex **1** was discussed. According to Figure 2b, the weightloss of complex **1** is 23.8% continuously from 25 °C to 212 °C, which is related to removal of four lattice DMF units along with three coordinated water molecules, the framework could be thermally stable up to 340 °C. Inspired via its latent porosity along with appropriate size of pore, we were encouraged to explore the microporous properties of the material. Complex **1** was assessed for 5 hours at 313 k under the condition of high vacuum after full exchange of acetone, resulting in solvent removal or activation for **1a**. Obviously, complex **1a** maintains its microporous properties, because the characteristic peaks are fundamentally consistent with the pattern of simulated XRD (Figure 2a).[19] After removing solvent molecules from the newly established framework, some displacements are expected to be discovered between **1** and **1a**. In addition, the TGA analysis of **1a** confirmed that there was no lattice or coordinated solvents in the framework of **1a**, which is evidenced by the absence of obvious weight loss between the temperatures of 25 and 367 °C. According to Figure 2c, at 77 K, the adsorption isotherm of N_2 shows that compound **1a** has a type I adsorption isotherm and there is a mild lag between desorption along with adsorption, it can use the dynamics characteristics of frame and multi-channel explanation. N_2

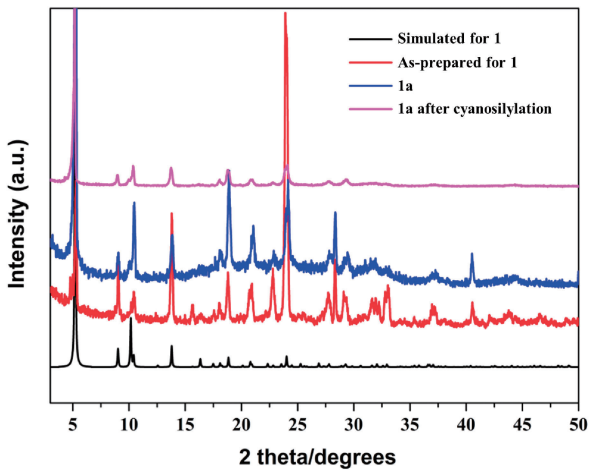

(a)

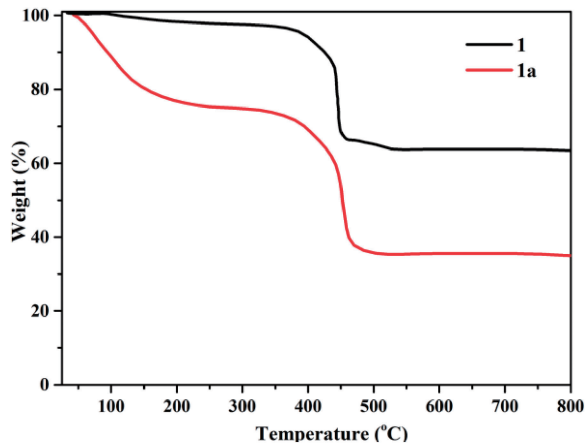

(b)

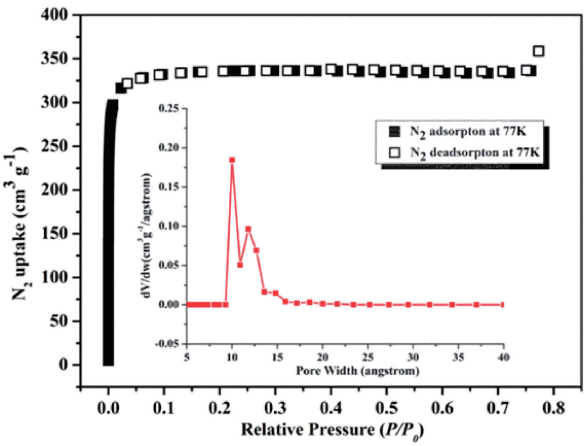

(c)

Figure 2. (a) **1** PXRD mode. (b) **1a** and **1** TGA curves. (c) **1a** data of N_2 adsorption.

adsorption capacity was up to 342 cm^3/g at 1 atm along with 77 K (Figure 2c). The estimated apparent Brunauer–Emmett–Teller (BET) surface area as well as the Langmuir surface area are 1100 along with 1477 m^2/g, respectively. The distribution ranges of pore size were between 10 and 12 Å. These results are the same as those of thermal stability along with crystal structure. It shows that the **1a** skeleton structure remains after solvent removal.

Table 1. Catalyst **1a** conditions optimization and **1** comparative test.

Entry	Cat. (mol%)	TMSCN	Temp. (°C)	Conv.[a]/%
1	0	2eq	40	36.6
2	1	2eq	40	65.2
3	1	2eq	rt	76.6
4	0.5	2eq	rt	96.5
5	0.1	2eq	rt	98.5
6	0.1 (**1**)	2eq	rt	38.2

[a]Determined via GC on the basis of carbonyl substrate.

Catalytic Properties of 1a. In considering the complex **1a** has coordinated unsaturated metal centers (UMCs) along with a large channel, it can be utilized as a latent Lewis acid catalyst for the cyanation of carbonyl compounds and tested for catalytic performance. Model experiments were carried out using benzaldehyde as a typical carbonyl under solvent-free conditions by changing the amount and temperature of catalyst. As seen in Table 1, complex **1a** indicated good activity, providing 98% benzaldehyde conversion at room temperature in one day, and the lowest catalyst loading of 0.1 mol% K, which is the highest activity of catalysis in cyanosilylation in a quantity of only 1/15 of Cr-MIL-101 (1.5 mol% Cr-active site).[20] In addition, **1a** as the catalyst does not require dichloromethane, but catalyst Cr-MIL-101 does. Only two hours later, **1a** was removed through filtration and reaction was completely stopped, and only 45% conversion was provided by standing for about 15 hours. This indicated that there was no homogeneous catalyst within the solution of reaction, and **1a** was a real heterogeneous catalyst. The K^+ ion concentration in the filtrate was determined via inductive coupled plasma emission spectrometry (ICP), which shows a value of 12 μM, indicating little K^+ ion leached into the reaction solution.

Under the conditions of optimization (2 equivalent TMSCN, catalyst 0.1 mol% and at room temperature), nine carbonyl substrates such as cyclic ketones, and aliphatic as well as aromatic aldehydes were cyanated. Results are gathered in Table 2, which revealed that the reaction has extensive applicability to a variety of substrates. Under the standard conditions, aromatic aldehydes bearing electron-effect (electron-withdrawing NO_2 and electron-donating CH_3) or distinct substituents were used. After about 9–12 hours of reaction, the yield of the product was over 90%. However, under the standard conditions, aliphatic aldehydes along with ketones usually have lower efficiency of catalysis than the aromatic aldehydes because of their inherent decreased reactivity. After a long reaction time (two days), cyclobutanone conversion was only up to 83%. In order to study and explain the open K^+ site fine activity of the catalysis, **1a** and **1** activities were detected under the same conditions of reaction. Cyanation reaction conversion rates of 40.3% along with 38.2% were acquired, which is similar to the conversion rate with no catalyst, which may be because of the saturation geometry of the whole K^+ ions within **1**. The results also show that the unsaturated K^+ coordination within **1a** has an important function in the process of catalysis.[21–23] In addition, the PXRD pattern of complex **1a** after the cyanosilylation reaction

Table 2. The cyanosilylation of various carbonyl compounds with TMSCN.

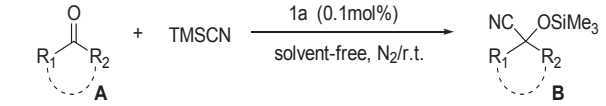

R_1 = Arkyl, Alkye; R_2 = H

Entry[a]	R1	R2	t/h	Conv.[b]/%
1	Ph	H	12	98
2	2-$CH_3C_6H_4$	H	12	93
3	4-$CH_3C_6H_4$	H	12	94
4	4-$NO_2C_6H_4$	H	9	99
5	n-Propyl	H	30	90
6	2-Furyl	H	34	95
7	$(CH_2)_4$	H	40	81
8	1-Naphthyl	H	40	76
9	9-Anthryl	H	48	0

Reaction conditions: [a]Me_3SiCN (1.0 mmol), aldehyde (0.5 mmol), **1a** of 0.1 mol%, at room temperature, under an atmosphere of N_2. [b]Determined via GC on the basis of the carbonyl substrate.

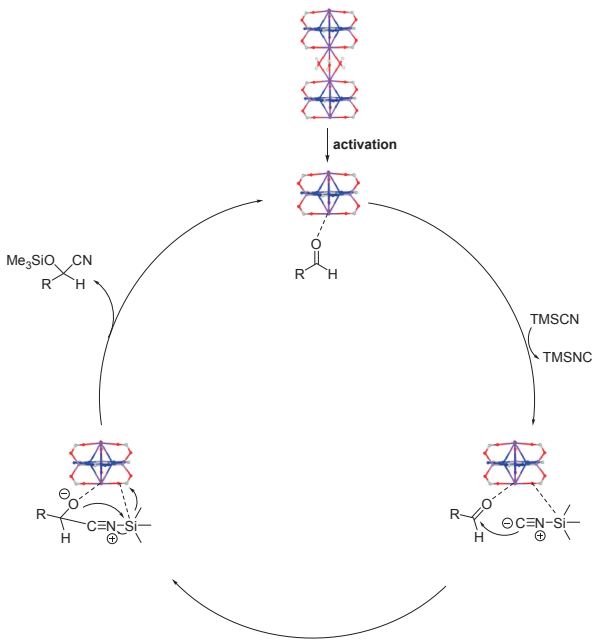

Scheme 1. The mechanism of **1a** carbonyl compound catalytic cyanation is proposed.

has also been acquired, which reveals a good match with that of the freshly prepared **1a**, showing its framework stability in the catalytic process (Figure 2a).

On the basis of the experimental results and reports in the literature, a rational reaction mechanism was put forward to explain the process of cyanation catalyzed by **1a**. The unstable water molecules within the **1a** channels were dislodged via heating to lay bare the metal centres of unsaturation. With coordinated K centres of unsaturation to active aldehydes, reaction with TMSCN occurred (Scheme 1). Using aldehydes to displace products, the catalysts activate continually aldehydes for the next cycle of catalysis.

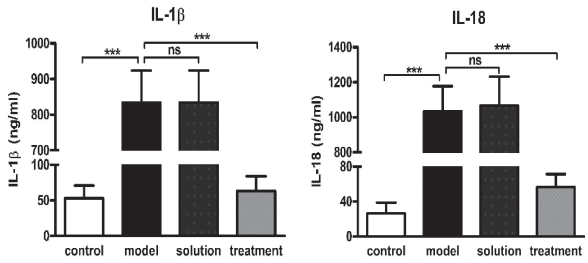

Figure 3. Reduced level of IL-18 and IL-1β in human brain microvascular endothelial cells after compound treatment. OGD was established in the hCMEC/D3 cells, followed by compound treatment. Then, we collected cell supernatant and level of pro-inflammatory IL-18 along with IL-1β was measured via ELISA detection.

Compound Reduced the Expression of IL-1β and IL-18. The pro-inflammatory cytokine expression level of IL-18 and IL-1β reflect inflammatory response in vivo. Usually, the excessive increase of pro-inflammatory cytokines IL-18 and IL-1β promote mucosa inflammation, which then accelerates the occurrence of chronic inflammation. Thus, in this experiment, the pro-inflammatory cytokines IL-18 and IL-1β were measured via ELISA assay one day after compound treatment. According to the results of Figure 3, in the OGD group, there was significant increased level of IL-18 and IL-1β compared with the control group, while, in the compound treatment group, the increased level of pro-inflammatory cytokines was obviously reduced, which is almost back to the normal level.

Compound Reduced the Production of ROS in Microvascular Endothelial Cells. The previous results indicated the compound could reduce the production of the inflammatory cytokines. Next, we further wanted to explore the relationship between the compound and the ROS production in the cells. After the construction of the oxygen-glucose deprivation model (OGD) in hCMEC/D3 microvascular endothelial cells of human brain, the compound was exposure to cells at a specified concentration for one day. ROS related gene expression was determined via RT-PCR. According to the results of Figure 4. The oxygen-glucose deprivation model could lead to a significant increase of the ROS level in the cells, that is significantly distinct with matched group ($p < 0.005$). After treating with compound, the up-regulated level of ROS was reduced, almost reaching control group level. The result revealed that the compound could inhibit the inflammatory condition of the human brain microvascular endothelial cells. In addition, compared with the MOFs reported previously, the synthetic MOF in this study showed stronger induction activity on the ROS production.[24]

Compound Reduced the Relative Expression of the ROS Related Genes. In the above research, we have demonstrated that this compound could inhibit production of ROS in human brain microvascular endothelial hCMEC/D3 cells. However, the detailed mechanism was still unknown, thus, in this experiment, we further wanted to explore the relative expression of *gp91* and *gp22*, which is reported to have a strong relationship with the production of the ROS in human brain microvascular endothelial. According to the results of Figure 5, we can observe that there was a significant increased level of the *gp91*

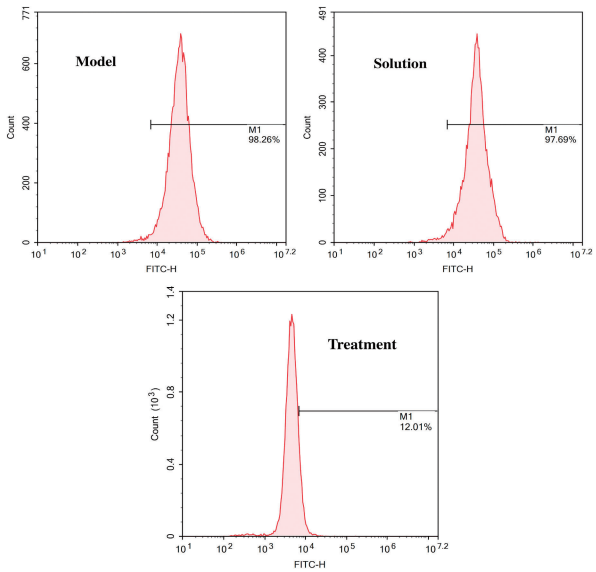

Figure 4. ROS production within hCMEC/D3 cells decreased after combined treatment. OGD was established in the hCMEC/D3 cells, followed by the compound treatment. The ROS level in the human brain microvascular endothelial cells was detected by ROS detection.

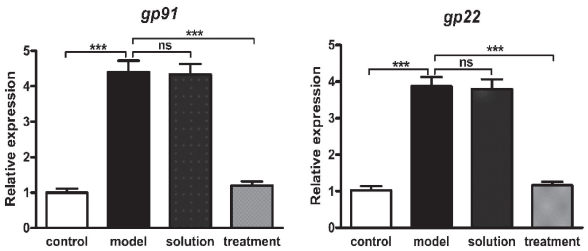

Figure 5. Reduced *gp91* and *gp22* expression level in human brain microvascular endothelial cells after compound treatment. OGD was established in the cells of hCMEC/D3, followed via the compound treatment. The expression level of the *gp91* and *gp22* in the cells of hCMEC/D3 was determined via RT-PCR.

and *gp22* expression level in the hCMEC/D3 cells, which also explains the high level of ROS in the cells. After the treatment via compound with the indicator concentration, *gp91* and *gp22* expression level was obviously reduced, compared with the model group.

Compound Prevents Neurological Deficit. After the previous *in vitro* study, we have revealed the protective effect of the compound in human brain microvascular endothelial cells by reducing the production of ROS. Subsequently, the treatment activity and prevention ability of the compound in the rat model was evaluated with the neurological deficit score. In Table 3, we can see that the neurological deficit score was reduced to 6.12 ± 2.75, which is significantly lower than the score in control groups ($p < 0.05$). The results showed that the compound had a good protective effect within the rat model.

3. Conclusion

In conclusion, we have generated a novel porous metal-organic framework by corresponding K(I)and Mn(II) salts and hetero-donor organic ligand 5-(1H-tetrazol-5-yl)isophthalic acid (H_3TZIA) solvothermal condition in water and DMF mixed solvent. X-ray single crystal study shows that K^+ ions were immobilized on the surface of pores via trinuclear Mn^{2+}–tetrazole coordination motif. The resulting activated **1a** has been explored in detail by BET analysis to probe its porosity. The removal of water molecules in order to generate **1a** makes it possible for K^+ ions to be applied as an efficient and size-selective multiphase catalyst for solvent-free cyanosilylation of acetaldehyde under mild conditions. The ELISA assay of IL-18 along with IL-1β indicated that compound could reduce the inflammatory level in human brain microvascular endothelial hCMEC/D3 cells. Besides, the ROS detection and RT-PCR results revealed the compound could also inhibit ROS production via reducing the ROS related gene expression. Finally, the protective effect of the compound in an animal model was evaluated, which suggested the excellent prevention activity of compound *in vivo*.

Table 3. Neurological deficit scores in animals before and after treatment.

Group	Pre-treatment score	Post-treatment score	Score difference
Control group (n = 30)	21.78 ± 6.75	21.65 ± 6.42	0.21 ± 0.63
Treatment group (n = 30)	22.03 ± 6.86	6.12 ± 2.75	16.92 ± 4.35
t	0.5021	6.7612	6.1249
P	>0.05	<0.05	<0.05

4. Experimental

Chemicals and Measurements. Solvents, reagents as well as the raw materials were all purchased from commercial sources and could be utilized with no further purification. With a Nicolet Avatar 360 FT-IR spectrophotometer we determine FT-IR spectra. The thermogravimetric analysis was performed under nitrogen flow with a Q50 TGA (TA) thermal analyzer, with a heating rate of 5 °C·min^{-1}. Powder X-ray diffraction patterns (PXRD) of samples of bulk were measured at room temperature on a MiniFlex (Cu Kα, λ = 1.5418 Å). GC analysis was carried out on an Agilent 7890B GC analyzer. The gas adsorption isotherms (N_2) at low pressure (up to 1 bar) were detected by porosity analyzer along with ASAP 2020 specific surface area.

Preparation and Characterization of $\{(Me_2NH_2)[Mn_3K_2(TZIA)_3(H_2O)_3]\cdot(DMF)_4\}_n$ (1). We synthesized complex **1** via $MnCl_2\cdot 4H_2O$ using 23.79 mg and 0.10 mmol, $KF\cdot 2H_2O$ of 14.10 mg and 0.15 mmol as well as H_3TZIA and 23.40 mg and 0.10 mmol solvothermal reaction in the mixed solvent of 2 mL H_2O, *N* and *N*-dimethylformamide (7 mL, DMF) for three days at 140 °C. We acquired light yellow crystals with block-shape. After filtration and separation from the mother solvent, we washed the crystals with anhydrous DMF three times, then dried it in air. The yield was approximately 62% on the basis of H_3TZIA. Anal. Calcd for $C_{41}H_{51}K_2Mn_3N_{17}O_{19}$ (**1**): C, 37.06; H, 3.87; N, 17.92%; found: C, 37.26; H, 3.99; N, 17.94%.

With an Oxford Xcalibur E diffractometer we acquired compound **1** X-ray data. CrysAlisPro software was used to analyze

Table 4. Compound **1** parameters of crystallography and refinement details.

Empirical formula	$C_{27}H_{15}K_2Mn_3N_{12}O_{15}$
Formula weight	990.51
Temperature/K	386.3
Crystal system	hexagonal
Space group	$P6_3/m$
a/Å	19.336(2)
b/Å	19.336(2)
c/Å	9.989(4)
α/°	90
β/°	90
γ/°	120
Volume/Å^3	3234.2(14)
Z	2
ρ_{calc}g/cm^3	1.017
μ/mm^{-1}	0.755
Data/restraints/parameters	1735/6/103
Goodness-of-fit on F^2	1.254
Final R indexes [$I \geqq 2\sigma(I)$]	$R_1 = 0.0987$, $\omega R_2 = 0.3033$
Final R indexes [all data]	$R_1 = 0.1119$, $\omega R_2 = 0.3127$
Largest diff. peak/hole/e Å^{-3}	1.15/−0.68
CCDC	1952188

the strength data, then convert strength data into hkl files. Based on the direct method, a primitive structure model was established using the SHELXS program, and modified via SHELXL-2014 based on the least square approach. All non-H atoms were mixed with the anisotropic parameters, and all the H atoms were geometrically fixed on their linked C atoms via utilizing the AFIX commands. Table 4 exhibits the parameters of crystallography along with the information of the numerical values of compound **1** after recombination.

Cell culture and MOF Treatment. Human brain microvascular HCMEC/D3 endothelial cells were purchase from American Type Culture Collection, and then cultured in ATCC-formulated RPMI-1640 culture medium. 2%L-glutamine, 100 U/ml penicillin-streptomycin solutions (Gibco, Life Technologies) as well as 10% (v/v) heat-inactivated fetal bovine serum (FBS) were added to the medium. The cells were cultured in an incubator at 37 °C along with 5% CO_2. The culture medium was replaced when the cells reached 80% confluence. The MOF was dissolved in DMSO to the concentration of 1 mg/mL for storage, before experiment the MOF solution was thoroughly dissolved in PBS to the indicated experimental concentration.

ELISA Assay. To detect the pro-inflammatory cytokines in hCMEC/D3 cell lines after complex treatment, IL-18 and IL-1β ELISA detection assay was carried out. We performed the experiment under the guidance of the manufacturer's protocols with some modifications. In brief, hCMEC/D3 endothelial cells were inoculated into a 96 well plate and then the oxygen-glucose deprivation model (OGD) was constructed. The compound was used for 24 h treatment. After that, we collected the supernatant of cell and the level of pro-inflammatory IL-18 and IL-1β was acquired by ELISA detection. All the plates were washed and added to a biotin-conjugated antibody for 2 h, then the absorbance of each well was measured at 450 nm. This experiment was carried out three or more times, the results were showed as mean ± SD.

ROS Detection. After treated with the compound at the indicated concentration, the ROS level in the cells was detected by ROS detection kit according to the instruction of the protocols. In brief, human brain microvascular endothelial cells hCMEC/D3 were inoculated into a 96 well plate and then the oxygen-glucose deprivation model (OGD) was constructed. The compound was added for treatment for the indicated time, followed by 20 μM DCFH-DA solution addition for 30 min cell incubation at 37 °C in the dark. Then, PBS was used to wash cells three times and then the cells were harvested. An ROS detection kit was used for the ROS measurement, the absorbance in each group was detected by flow cytometry (BD Via, New Jersey, USA) at 488/530 nm and analyzed with FlowJo7.6 software.

RT-PCR of *gp91* and *gp22*. Human brain microvascular endothelial cells HCMEC/D3 were inoculated into a 96 well plate and then the oxygen-glucose deprivation model (OGD) was constructed before the compound treatment. Subsequently, the relative expression of the *gp91* and *gp22* in cells were examined by RT-PCR according to the protocols. Briefly, total RNA in cells was extracted with TRIzol and quantified with the detection kit. Next, a One-Step RT-PCR kit was utilized for the RNA reverse-transcribing into cDNA, and the RT-PCR was carried out utilizing SYBR® Premix Ex Taq™ kit (Takara). Finally, we calculated relative expression quantification of *gp91* and *gp22* with $2^{-\Delta\Delta CT}$ approach after the standardization of *gapdh* mRNA.

Neurological Deficit Score. The experimental animals were randomly divided into a control group and a treatment group. The neurological function of the experimental animals was evaluated before and after the compound treatment. The greater the difference between the two groups, the better the treatment effect and the better recovery of nerve function. According to the physiological functions of the experimental animals, the evaluation of the therapeutic effect of the compound evaluation was divided into: Complete recovery, no obvious sequelae, neurological function score reduced by >90%; Improved, with slight sequelae, neurological function score decreased >65%; Ineffective, with no recovery or improvement.

Statistical Analysis. All the results in this research were collected from the independent experiments of three or more repeats. All data were analyzed by Graphpad Prism 5.0 software and expressed as average value (±) standard deviation (SD). Two-way t-test was used for comparing differences of the two groups. One-way ANOVA was applied to compare more than three groups. When $p < 0.05$, it is estimated that there is statistical difference.

Reference

# Authors are contributed equally to this work.

1 P. Wang, P. Qiao, H. Xing, R. Zhang, E. Lingling, H. Liu, *J. Nanosci. Nanotechnol.* **2020**, *20*, 1417.

2 D. Zhang, H. Q. Zhang, S. Zhao, Z. G. Li, S. X. Hou, *Int. J. Electrochem. Sci.* **2019**, *14*, 4659.

3 S. Guo, R. Chen, H. Li, T. Zhang, Y. Liu, *Int. J. Softw. Eng. Knowl. Eng.* **2019**, *29*, 139.

4 W. Zheng, C. Liu, *Anatol. J. Cardiol.* **2019**, *22*, 102.
5 X. Feng, Y. Q. Feng, N. Guo, Y. L. Sun, T. Zhang, L. F. Ma, L. Y. Wang, *Inorg. Chem.* **2017**, *56*, 1713.
6 X. Feng, R. F. Li, L. Y. Wang, S. W. Ng, G. Z. Qin, L. F. Ma, *CrystEngComm* **2015**, *17*, 7878.
7 Y. Xiong, Y. Z. Fan, R. Yang, S. Chen, M. Pan, J. J. Jiang, C. Y. Su, *Chem. Commun.* **2014**, *50*, 14631.
8 Y. S. Wei, X. P. Hu, Z. Han, X. Y. Dong, S. Q. Zang, T. C. W. Mak, *J. Am. Chem. Soc.* **2017**, *139*, 3505.
9 X. Feng, X. L. Ling, L. Liu, L. Y. Wang, S. W. Ng, B. Y. Su, *Dalton Trans.* **2013**, *42*, 10292.
10 X. Feng, Y. Q. Feng, L. Liu, L. Y. Wang, H. L. Song, S. W. Ng, *Dalton Trans.* **2013**, *42*, 7741.
11 J. Qian, F. Jiang, K. Su, J. Pan, Z. Xue, L. Liang, P. P. Bag, M. Hong, *Chem. Commun.* **2014**, *50*, 15224.
12 U. Schubert, *Chem. Soc. Rev.* **2011**, *40*, 575.
13 J. J. Song, F. Gallou, J. T. Reeves, Z. Tan, N. K. Yee, C. H. Senanayake, *J. Org. Chem.* **2006**, *71*, 1273.
14 Y. Kikukawa, K. Suzuki, M. Sugawa, T. Hirano, K. Kamata, K. Yamaguchi, N. Mizuno, *Angew. Chem., Int. Ed.* **2012**, *51*, 3686.
15 X. Cui, M. C. Xu, L. J. Zhang, R. X. Yao, X. M. Zhang, *Dalton Trans.* **2015**, *44*, 12711.
16 A. Bhunia, S. Dey, J. M. Moreno, U. Diaz, P. Concepcion, K. Van Hecke, C. Janiak, P. Van Der Voort, *Chem. Commun.* **2016**, *52*, 1401.
17 S. Neogi, M. K. Sharma, P. K. Bharadwaj, *J. Mol. Catal. A: Chem.* **2009**, *299*, 1.
18 T. Ladrak, S. Smulders, O. Roubeau, S. J. Teat, P. Gamez, J. Reedijk, *Eur. J. Inorg. Chem.* **2010**, 3804.
19 D. M. Chen, X. J. Zhang, *CrystEngComm* **2019**, *21*, 4696.
20 Z. Zhang, J. Chen, Z. Bao, G. Chang, H. Xing, Q. Ren, *RSC Adv.* **2015**, *5*, 79355.
21 B. Bai, J. Li, *ACS Catal.* **2014**, *4*, 2753.
22 H. Shimokawa, Y. Kurihara, H. Kusaba, H. Einaga, Y. Teraoka, *Catal. Today* **2012**, *185*, 99.
23 X. Yuan, S. Fan, L. Zhao, H. T. Kim, *Energy Fuels* **2016**, *30*, 2492.
24 N. Takano, *J. Appl. Physiol.* **1988**, *64*, 2631.

